


Transcriptional heterogeneity of stemness phenotypes in the ovarian epithelium

Lauren E. Carter^{1,2,3}, David P. Cook^{1,2,3}, Curtis W. McCloskey^{1,2}, Melanie A. Grondin^{1,2}, David A. Landry^{1,2}, Tiffany Dang^{1,2}, Olga Collins^{1,2}, Lisa F. Gamwell^{1,2}, Holly A. Dempster^{1,2} & Barbara C. Vanderhyden^{1,2}  [✉]

The ovarian surface epithelium (OSE) is a monolayer of epithelial cells surrounding the ovary that ruptures during each ovulation to allow release of the oocyte. This wound is quickly repaired, but mechanisms promoting repair are poorly understood. The contribution of tissue-resident stem cells in the homeostasis of several epithelial tissues is widely accepted, but their involvement in OSE is unclear. We show that traits associated with stem cells can be increased following exposure to the cytokine TGF β 1, overexpression of the transcription factor *Snai1*, or deletion of *Brca1*. We find that stemness is often linked to mesenchymal-associated gene expression and higher activation of ERK signalling, but is not consistently dependent on their activation. Expression profiles of these populations are extremely context specific, suggesting that stemness may not be associated with a single, distinct population, but rather is a heterogeneous cell state that may emerge from diverse environmental cues. These findings support that the OSE may not require distinct stem cells for long-term maintenance, and may instead achieve this through transient dedifferentiation into a stem-like state.

¹Cancer Therapeutics Program, Ottawa Hospital Research Institute, Ottawa, ON, Canada. ²Department of Cellular and Molecular Medicine, University of Ottawa, Ottawa, ON, Canada. ³These authors contributed equally: Lauren E. Carter, David P. Cook. ✉email: bvanderhyden@ohri.ca

It is thought that stem cell populations are responsible for long-term maintenance of many adult tissues. The characterization of stem cells associated with epithelial tissue maintenance has been an active field of research for the past few decades. While several distinct stem cell populations have been functionally described, such as an LGR5 + population at the base of intestinal crypts¹, it is unclear if all epithelial tissues are maintained by such defined populations. For example, it has been shown that following stem cell depletion, differentiated airway epithelial cells can dedifferentiate and become functional multipotent stem cells². It is also unclear if stem cells are necessarily required to maintain epithelial tissues comprising a single cell type, as some baseline capacity for proliferation could maintain the entire tissue. In the mesothelium, for example, there have been reports of putative stem/progenitor cells for over two decades, but a well-defined stem cell population has yet to be identified³.

The ovarian surface epithelium (OSE) is a promising tissue for studying stemness dynamics in tissue maintenance. It is a monolayer of cells surrounding the ovary and, during each ovulation, this tissue is ruptured to facilitate release of an oocyte. Afterwards, the OSE layer is rapidly repaired^{4–7}. Post-ovulatory wound repair is a poorly understood process despite ovulation being the primary non-hereditary risk factor for ovarian cancer.

Several putative OSE stem cell populations have been described, each defined by different cell surface markers, including ALDH1A1, LGR5, LY6A (Sca-1), and more^{8–11}. However, relationships between the populations described in these studies are still unclear, with little known about co-expression or mutual exclusivity of markers. Further, it is unclear if these populations are static or can emerge from differentiated OSE in response to ovarian dynamics. We have previously shown that, like the mammary epithelium¹², induction of an epithelial-to-mesenchymal transition (EMT) can transiently promote features of stem cells (stemness) in differentiated OSE¹⁰. This is particularly relevant in the context of ovulation, as the EMT is thought to be an important component of wound repair and the EMT-promoting cytokine TGFβ1 is present in follicular fluid, bathing adjacent OSE at ovulation^{10,13}. It is also secreted by macrophages at the ovulatory wound and granulosa cells during follicular development^{14,15}.

Here, we further demonstrate that features of stemness can be altered in OSE cells. Profiling gene expression of different populations with enhanced stemness, we demonstrate that some features are relatively common, including EMT-associated expression patterns and enhanced activity of ERK and NFκB signaling, but global expression profiles are widely variable and stemness is not exclusively dependent on these common features. Together, this work supports that OSE tissue maintenance may not require a distinct stem cell population, but can emerge in response to their environment.

Results

CD44 is a marker of EMT-associated stemness in OSE cells. We have previously demonstrated that mouse OSE (mOSE) cells undergo an EMT through canonical SMAD signaling when exposed to TGFβ1 and acquire stem cell characteristics^{10,16}. To confirm these findings, we first assessed the ability of TGFβ1-treated mOSE cells to form self-renewing spheroids in suspension culture. Treated cells formed over twice as many primary spheroids and, when dissociated and cultured, were more efficient at successfully generating secondary spheroids, confirming their capacity for self-renewal (Fig. 1a). Morphologically, mOSE spheres were large and compact, with no difference in their size regardless of whether they had been treated with TGFβ1 (Fig. 1b). This suggests that the phenotype is not simply the result of

increased proliferation rates, but rather reflects an increased ability for clonogenic growth. Consistent with this, we have previously shown that TGFβ1 reduces the growth rate of mOSE¹⁰.

To validate this enhanced stemness in human cells, we also performed these experiments on primary cultures of human OSE (hOSE) cells. Since hOSE cultures have a low proliferation rate in vitro, we used methylcellulose-based suspension culture to immobilize the cells and minimize the impact of aggregation in our quantifications. While these conditions, along with the slower proliferation, resulted in smaller spheroids, TGFβ1-treated hOSE cells formed 3 times as many spheroids as untreated cells (Fig. 1c).

To determine if this enhanced stemness is associated with the expression of previously reported markers of OSE stem cells, we measured their expression throughout 7 days of TGFβ1 treatment in mOSE cells. *Aldh1a1*, *Lgr5*, and *Nanog* did not increase with TGFβ1 treatment, and in some cases decreased over time (Supplementary Fig. 1). While this does not preclude the possibility of these genes being valid markers of stem cell populations in vivo, these results suggest that their regulation is independent from TGFβ1-associated stemness.

We next assessed the expression of a larger panel of markers from a commercial “Stem Cell Marker” qPCR array in order to identify putative markers that are associated with this stemness (Fig. 1d). This identified several highly upregulated markers following 7 days of TGFβ1 treatment, including *Ncam1* (14-fold), *Cd44* (13-fold), and *Ascl2* (6-fold) (Fig. 1d). CD44 has long been associated with stemness in mammary epithelial cells¹⁷ and more recently in the oviductal epithelium¹⁸. We first validated CD44 RNA and protein levels throughout TGFβ1 treatment and found that it increases after four days of treatment (Fig. 1e; Supplementary Fig. 2). We then stained both control and TGFβ1-treated spheroids for CD44 and Ki67 to assess the distribution of proliferation and this putative stemness phenotype within spheroids (Fig. 1f; Supplementary Fig. 3). CD44 was detectable in many control spheroids but was expressed only in rare cells throughout the population. Cells comprising TGFβ1-treated spheroids, however, ubiquitously expressed CD44. Proliferative cells were diffuse throughout the spheroids with no clear association with spatial location within the spheroid or relative to CD44 + cells. Both CD44 expression patterns are consistent with the possibility that CD44 expression enriches for stem-like cells capable of seeding clonogenic growth of spheroids. To test this, we sorted CD44^{high} cells from TGFβ1-treated mOSE by fluorescence-activated cell sorting (FACS). When placed in suspension culture, CD44^{high} cells formed approximately 2.5 times as many spheroids compared to CD44^{low} cells (Fig. 1g).

Transcriptional profiling of mOSE stemness. We next sought to define a global profile of stemness, beyond a small number of markers. Spheroids themselves have been demonstrated to be enriched with stem/progenitor populations and challenge cells to exhibit stemness traits, including clonogenic growth and self-renewal^{19–21}. Since untreated mOSE cultures are capable of sphere formation, albeit at a lower frequency than TGFβ1-treated mOSE cells, we reasoned that the transcriptional profile of these spheroids may represent an intrinsic stemness program, independent from exogenous factors. To compare this with TGFβ1-induced stemness, we performed RNA-seq on mOSE cells cultured as a monolayer or as spheroids, each with and without TGFβ1 treatment.

Untreated mOSE cells cultured as spheroids exhibited striking differences from those cultured in a monolayer, with 4950 differentially expressed genes between the conditions ($p < 0.05$,

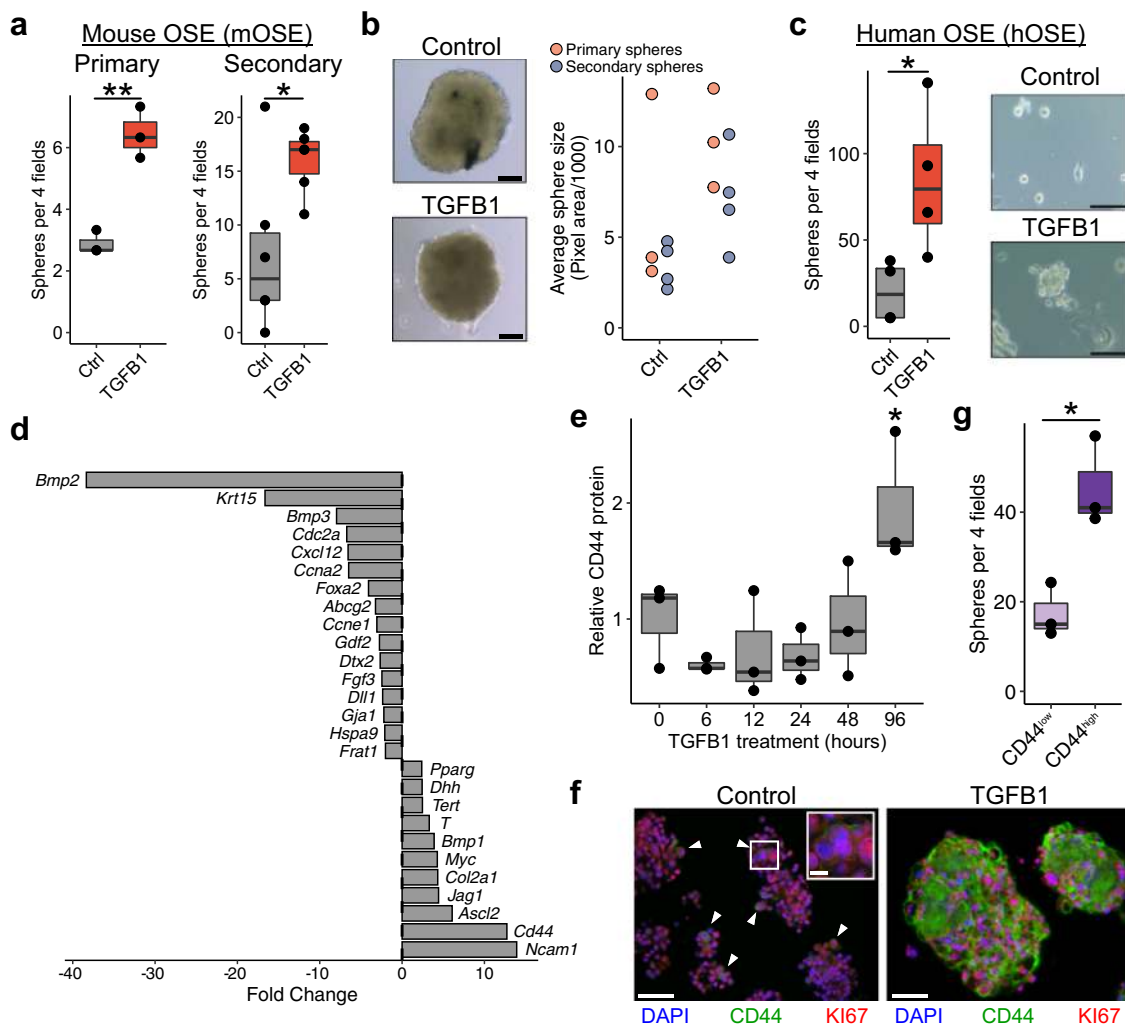


Fig. 1 TGFβ1 promotes stemness in the OSE. **a** Primary (left; $n = 3$) and secondary (right; $n = 5$) sphere-forming capacity of mOSE cells treated with TGFβ1 (10 ng/mL). Data points represent the average number of spheres per 4 fields of view for each replicate after 14 days of spheroid culture. **b** Left: Phase contrast images of control and TGFβ1-treated spheroids (left). Scale bar = 100 μm . Right: Relative sizes of spheroids in control and TGFβ1 conditions (primary spheroids $n = 3$; secondary spheroids $n = 4$). Each point on the plot represents the average size of spheroids from 4 fields of view for 4 separate wells. **c** Primary sphere-forming capacity of human OSE treated with TGFβ1 ($n = 4$). hOSE spheroids were cultured in methylcellulose to prevent aggregation. Spheroids were cultured for 28 days. Scale bar = 100 μm . **d** Fold change values for a panel of putative stem cell markers in mOSE treated with TGFβ1 for 4 days. **e** Relative protein quantifications of CD44 throughout a time course of TGFβ1 treatment in mOSE ($n = 3$). Quantifications represent Western blot pixel densitometry, normalized to B-actin and scaled to the mean intensity in untreated samples. A representative blot is included in Supplemental Fig. 2b. **f** Immunofluorescence co-stain of CD44 and Ki67 in control and TGFβ1-treated spheroids. White arrows highlight CD44+ cells in control spheroids. Scale bar = 100 μm , inset scale bar = 15 μm . Separate channels are shown in Supplementary Fig 3g. Primary sphere-forming capacity of CD44- and CD44+ mOSE cells ($n = 3$). All boxplots show median value (horizontal black line), estimated 25th and 75th percentiles, and whiskers represent 1.5 times the interquartile range. Linear regression models were used for all statistical tests. * $p < 0.05$, ** $p < 0.01$.

absolute log fold change >0.5) (Fig. 2a; Supplemental Data 1). Using an aggregate reference of GO terms, KEGG pathways, Reactome pathways, and MSigDB Hallmark gene sets from the Molecular Signatures Database (MSigDB)^{22,23}, we used gene set enrichment analysis (GSEA) to identify biological features associated with these changes (Fig. 2c; Supplemental Data 2). Spheroids were associated with decreased cell cycle, epithelial cell adhesion, and, interestingly, DNA repair. Along with these changes, spheroid culture activated expression of chemokine signaling and wound repair programs. We also note that CD44, which we had used as a selection marker for stemness in TGFβ1-treated mOSE, was also expressed over 4-fold higher in spheroids, whereas *Aldh1a1*, *Lgr5*, and *Ly6a* (*Sca-1*) were unchanged (Fig. 2b). We next used the PROGENy algorithm to infer changes in signaling pathway activity across these samples that

may be contributing to these differences. Spheroids were associated with increased activity of many signaling pathways, with the largest increases in Hypoxia, NFκB, and MAPK signaling (Fig. 2d). While GSEA results suggest several EMT-related changes, TGFβ1 and WNT signaling are interestingly reduced, suggesting that this EMT program may be activated through NFκB or ERK (Fig. 2d).

While TGFβ1 signaling was decreased in untreated spheroids when compared to monolayer cultures, exogenous TGFβ1 treatment of monolayers enhanced stemness, increasing the proportion of cells capable of forming self-renewing spheroids. While these results are seemingly contradictory, week-long exposure to exogenous TGFβ1 may activate similar expression programs through secondary effects or signaling crosstalk²⁴. We next assessed expression changes associated with TGFβ1

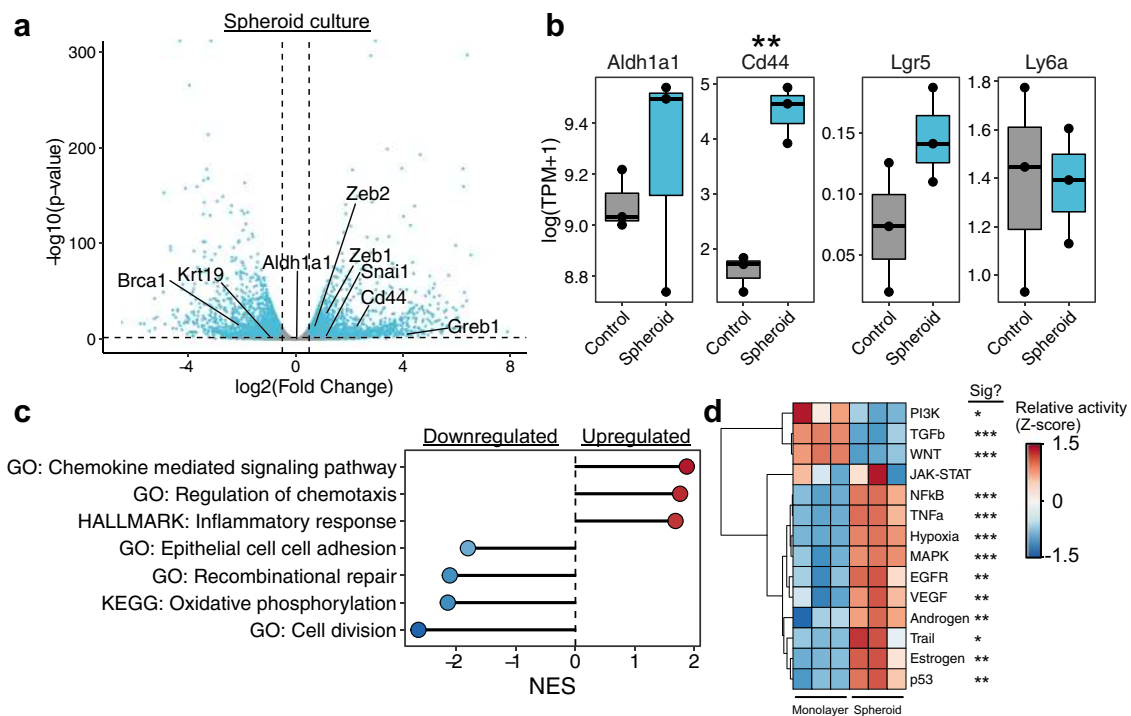


Fig. 2 Transcriptional profile of intrinsic mOSE stemness. **a** Plot showing the distribution of differentially expressed genes in mOSE cells cultured as spheroids for 14 days relative to a monolayer ($n = 3$). Each point corresponds to a single gene. Selected genes related to stemness and/or the EMT are highlighted on the plot. Dashed lines correspond to significance criteria (absolute log fold change >0.5 , $p < 0.05$). **b** Boxplots showing the expression values of putative mOSE stemness markers in mOSE cells cultured in a monolayer (Control) or as spheroids ($n = 3$). Boxplots show median value (horizontal black line), estimated 25th and 75th percentiles, and whiskers represent 1.5 times the interquartile range. **c** GSEA results for selected gene sets enriched in differentially expressed genes in mOSE spheroids. All gene sets are significantly enriched ($p < 0.05$) and normalized enrichment scores (NES) are shown. **d** Inferred pathway activity in monolayer- and spheroid-cultured mOSE cells. Linear models were used for statistical testing for **b** and **d**. * $p < 0.05$, ** $p < 0.01$, *** $p < 0.001$.

exposure. Treatment of monolayer cultures with TGF β 1 for 7 days resulted in 1508 differentially expressed genes ($p < 0.05$, absolute log fold change >0.5) (Fig. 3a; Supplemental Data 3). This involved the activation of EMT-associated gene sets as expected, as well as a reduction in oxidative phosphorylation (Fig. 3b; Supplemental Data 4). While TGF β 1 signaling was the only pathway inferred to have significantly altered activity, the estimated activity of EGFR and MAPK was higher in TGF β 1-treated cells ($p = 0.1$ and 0.06 , respectively) (Fig. 3c). Consistent with this, the GO term “ERK1 and ERK2 signaling cascade” was significantly enriched in upregulated genes following TGF β 1 treatment (Fig. 3b).

This suggests that TGF β 1 treatment initiates sequential or parallel signals similar to those present in spheroids. Consistent with this, untreated spheroids and TGF β 1-treated mOSE monolayers have a significant overlap in expression changes relative to untreated mOSE cells cultured as a monolayer, sharing 270 upregulated genes and 293 downregulated genes (Fisher exact $p = 3.0e-66$ and $2.8e-117$, respectively) (Fig. 3d). Conserved upregulated genes were strongly enriched for EMT-associated genes, NF κ B signaling, and angiogenesis (Fig. 3e). Interestingly, very few gene sets were enriched in the conserved downregulated genes, with only interferon response and substrate adhesion genes being enriched (Fig. 3e). We then explored the gene expression patterns of TGF β 1-treated spheres using a linear model with an interaction term to identify expression changes that were not simply the additive effects of TGF β 1 and spheroid culture (Supplementary Fig. 4a). We performed GSEA on genes ranked by the interaction coefficient of this model and found that TGF β 1-treated spheres were associated with higher expression of genes associated with EMT, MAPK/ERK, and inflammatory

pathways (Supplementary Fig. 4b). They also had notable differences in the expression of metabolic genes, with an increase in oxidative phosphorylation and reduced cholesterol biosynthesis. Together, these findings suggest that various responses may contribute to OSE stemness, including increased MAPK/ERK signaling, activation of inflammatory response pathways such as NF κ B and STAT, and EMT-associated gene expression.

Snail activation promotes a unique stemness program in mOSE cells.

Signaling pathways are highly pleiotropic and it is unclear if TGF β 1-enhanced stemness is activated from core EMT regulatory networks or alternative components regulated by TGF β 1. The EMT transcription factor *Snail* (Snail) was upregulated in both TGF β 1-treated mOSE cells and spheroids (Figs. 2a and 3a), and so to determine if EMT activation without exogenous cytokines could promote stemness, we derived mOSE cell lines with doxycycline-inducible Snail expression. Following Snail induction, cells had a higher sphere forming capacity than cells without doxycycline exposure, generating up to twice as many primary spheres and 3 times as many secondary spheres when passaged (Fig. 4a). Despite a higher sphere-forming efficiency, spheroid size was not different between control and Snail-overexpressing cells and the baseline proliferation rate of the cells was also unchanged (Supplementary Fig. 5a, b).

We next assessed the expression of the putative stem cell markers *Cd44* and *Sca-1*, which are both increased with TGF β 1 treatment, and found that Snail induction had no effect on their expression, suggesting that their validity as markers of stemness may be context specific. To determine if Snail induction activates similar expression patterns to TGF β 1-treated mOSE and

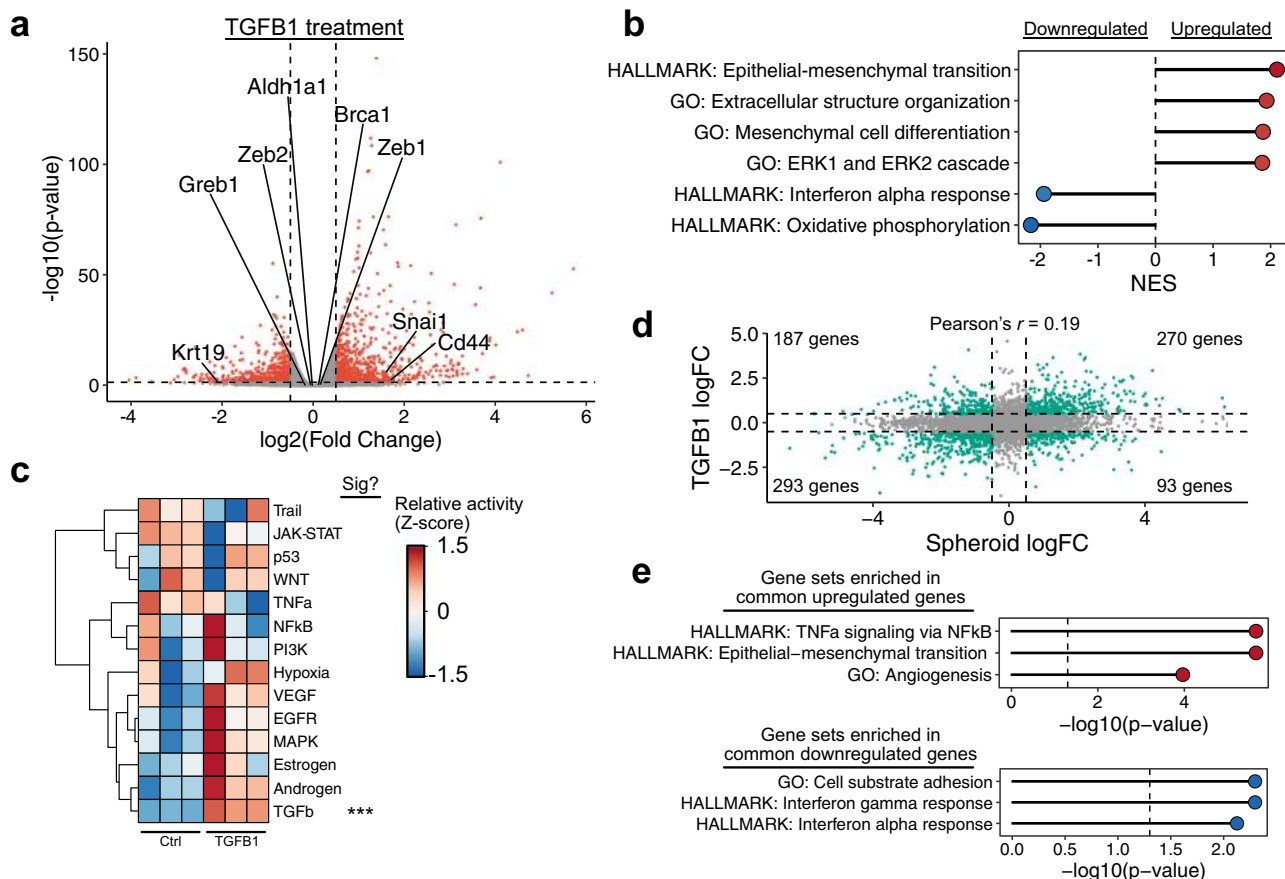


Fig. 3 TGFβ1 promotes a distinct stemness phenotype. **a** Plot showing the distribution of differentially expressed genes in monolayers of mOSE cells treated with TGFβ1 compared to untreated samples ($n = 3$). Each point corresponds to a single gene. Selected genes related to stemness and/or the EMT are highlighted on the plot. Dashed lines correspond to significance criteria (absolute log fold change >0.5 , $p < 0.05$). **b** GSEA results for selected gene sets enriched in differentially expressed genes following TGFβ1 treatment. All gene sets are significantly enriched ($p < 0.05$) and NES values are shown. **c** Inferred pathway activity in untreated and TGFβ1-treated mOSE cells. P -values were computed from the t statistic of a linear regression model and were adjusted using the Benjamini-Hochberg false discovery rate (FDR) method. **d** Plot comparing log fold-change values for spheroid-cultured and TGFβ1-treated mOSE. Dashed lines correspond to fold change cutoffs used to assess significance. **e** Plots showing gene sets enriched in commonly up- or downregulated genes following both TGFβ1 treatment and spheroid culture. P -values were calculated using a Fisher exact test and were adjusted using the Benjamini-Hochberg FDR method.

spheroids, including higher ERK and NFκB activity, we performed RNA-seq on these cells with and without doxycycline. Snail-induced changes were more modest than with TGFβ1 treatment or in spheroid culture, with only 85 upregulated and 44 downregulated genes ($p < 0.05$, absolute log fold change >0.5 ; Fig. 4b; Supplemental Data 5). Interestingly, inferred pathway activity scores associated with EGFR, NFκB, MAPK, and TGFβ1 were all unchanged following Snail induction (Fig. 4c). Further, no relevant gene sets associated with these pathways were enriched in the differentially expressed genes (Fig. 4d). The only gene sets associated with upregulated genes were largely related to cell morphology and extracellular matrix (ECM) remodeling (Fig. 4d; Supplemental Data 6). Consistent with TGFβ1-treated mOSE and spheroids, the MSigDB Hallmark “Interferon Alpha Response” was the only gene set enriched in the downregulated genes following Snail induction (Fig. 4d). We note that of the 85 upregulated genes following Snail induction, 13 are shared with those commonly regulated in TGFβ1 treatment and spheroids (Fig. 4e). These genes largely represent components of the ECM, including *Col18a1* and the metalloproteinases *Mmp9* and *Adamts4*. As the conditions share no consistently activated downstream signal that could be induced by ECM changes, these findings suggest that expression programs associated with

stemness phenotypes are heterogeneous. Given frequent enrichment of gene sets associated with a mesenchymal phenotype, stemness may consistently involve higher levels of these traits, which can emerge from variable expression patterns²⁵.

BRCA1 loss promotes EMT-independent stemness in mOSE.

Spheroids were associated with higher expression of many genes that were not similarly induced by TGFβ1 treatment. We noted that among spheroid culture-induced genes were several changes typically associated with ovarian cancer, including activation of the transcription factor *Pax8*, which is present in approximately 80% of ovarian tumors but not typically expressed in murine OSE²⁶; activation of *Greb1*, which promotes ovarian cancer growth²⁷; and loss of *Brca1*, which, along with *Brca2*, is mutated in approximately 22% of high-grade serous ovarian tumors. Interestingly, loss of BRCA1 has been associated with promoting dedifferentiation and activation of EMT expression patterns in mammary epithelial cells²⁸.

As the association between BRCA1 loss and stemness in the OSE had not been assessed, we next derived a primary mOSE line from *Brca1^{tm1Brn}* mice harboring floxed *Brca1* alleles. To determine if BRCA1 loss enhanced stemness in these cells, we

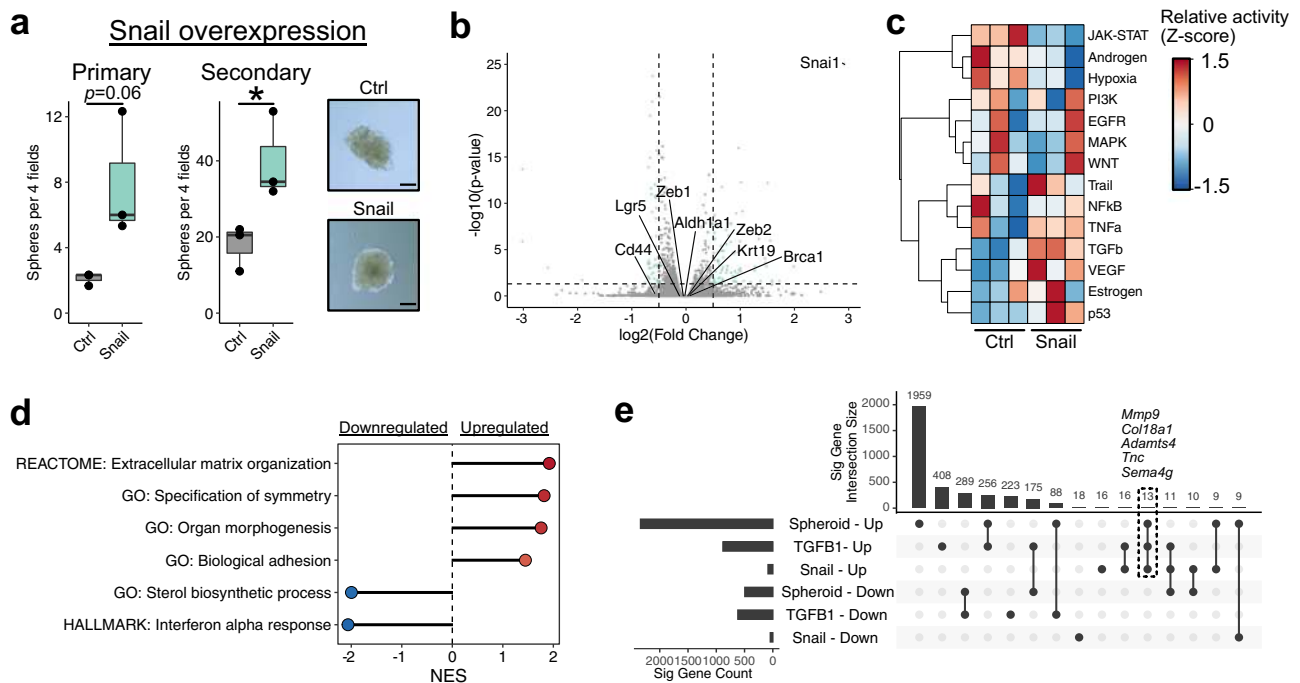


Fig. 4 Snail overexpression promotes stemness with minimal gene expression changes. **a** Primary (left) and secondary (middle) sphere forming capacity of mOSE cells overexpressing Snail ($n = 3$). Data points represent the average number of spheres per 4 fields of view for each replicate. Boxplots show median value (horizontal black line), estimated 25th and 75th percentiles, and whiskers represent 1.5 times the interquartile range. Right: Phase contrast images of control (inducible GFP) and Snail-overexpressing spheroids. Spheroids were cultured for 14 days. Scale bar = 100 μm . **b** Plot showing the distribution of differentially expressed genes following Snail overexpression. Each point corresponds to a single gene. Selected genes related to stemness and/or the EMT are highlighted on the plot. Dashed lines correspond to significance criteria (absolute log fold change >0.5 , $p < 0.05$). **c** Inferred pathway activity in control and Snail-overexpressing mOSE cells. P -values were computed from the t statistic of a linear regression model and were adjusted using the Benjamini-Hochberg FDR method. No pathway is significantly different between conditions. **d** GSEA results for selected gene sets enriched in differentially expressed genes following Snail overexpression. All gene sets are significantly enriched ($p < 0.05$) and NES values are shown. **e** UpSet plot showing overlaps in differentially expressed genes between all conditions assessed ranked by the condition/overlap with the largest number of genes. The top chart shows the intersection size for the conditions highlighted in the middle grid. A single, unconnected point corresponds to genes unique to only that condition. The total number of differentially expressed genes in each condition is shown in the left chart.

infected the cells with adenovirus containing either Cre recombinase (Ad-Cre) or GFP (Ad-GFP) as a control. Cre delivery, while not perfectly efficient, resulted in an approximately 60% reduction in BRCA1 levels across the population (Supplementary Fig. 6). When placed in suspension culture, cells with reduced BRCA1 formed over 5 times as many primary spheres and 3 times as many secondary spheres than control mOSE cells, suggesting that BRCA1 loss also enhances stemness in mOSE cells (Fig. 5a). There was no difference in the size of the spheres and BRCA1 deletion modestly decreased the growth rate of cells in monolayer culture ($p = 0.008$, linear regression on cell counts from days 1–5) (Supplemental Fig. 7a, b).

To assess if BRCA1 loss enhances stemness phenotypes in vivo, we crossed the *Brcal^{tm1Brn}* mice with *B6.129×1-Gt(ROSA)26Sor^{tm1(EYFP)Cos/J}* mice to generate a *Brcal^{fl/fl}YFP* mouse line, allowing us to track *Brcal*-null cells following exposure to Ad-Cre. These mice were injected intrabursally (IB) with Ad-Cre or PBS, and injected intraperitoneally (IP) with bromodeoxyuridine (BrdU). Ovaries were collected after a 30-day chase period and assessed for retention of the BrdU label and activation of the YFP reporter. Ad-Cre injection IB in *Brcal^{fl/fl}YFP* mice showed successful activation of the YFP reporter, compared to the PBS injection (Fig. 5b). When combining the IB injections with an IP BrdU injection, Ad-Cre treatment increased the number of label-retaining OSE cells (Fig. 5c, d). Given the high frequency of ovulations of the mouse ovary over the 30-day chase period, this increased label retention following BRCA1 loss is consistent

with BRCA1 deletion leading to expansion of quiescent stem-like cells in the OSE. Whether this is through expansion of an existing stem-like population or dedifferentiation of mOSE is unclear.

To determine if BRCA1 loss results in similar expression patterns to other conditions associated with stemness, we performed RNA-seq on mOSE cells isolated from these mice infected with Ad-Cre or Ad-GFP in vitro. BRCA1 loss resulted in a large shift in gene expression, with 1499 significantly upregulated genes and 1881 downregulated ($p < 0.05$, absolute log fold change >0.5 ; Fig. 6a; Supplemental Data 7). In mammary epithelium, the induction of EMT through *Brcal* deletion was presumed to be due to loss of BRCA1-mediated repression on the promoter of the EMT transcription factor *Twist1*. In contrast, we found that *Twist1* was approximately 8-fold lower in *Brcal*-null mOSE cells (Fig. 6a). There were also no EMT-associated gene sets enriched in upregulated genes. Rather, upregulated genes were largely enriched for gene sets associated with cell membrane transporters and downregulated genes were associated with cell cycle, oxidative phosphorylation, and DNA repair (Fig. 6b; Supplemental Data 8). *Brcal* deletion did not result in other features of stemness we observed in previous conditions, including activation of ERK and NFkB, and repression of interferon alpha response genes (Fig. 6c). *Brcal*-null cells were associated with reduced PI3K signaling and higher levels of estrogen signaling (Fig. 6c). Estrogen has been linked to EMT and stemness in other cell types²⁹, but this is presumed to be through

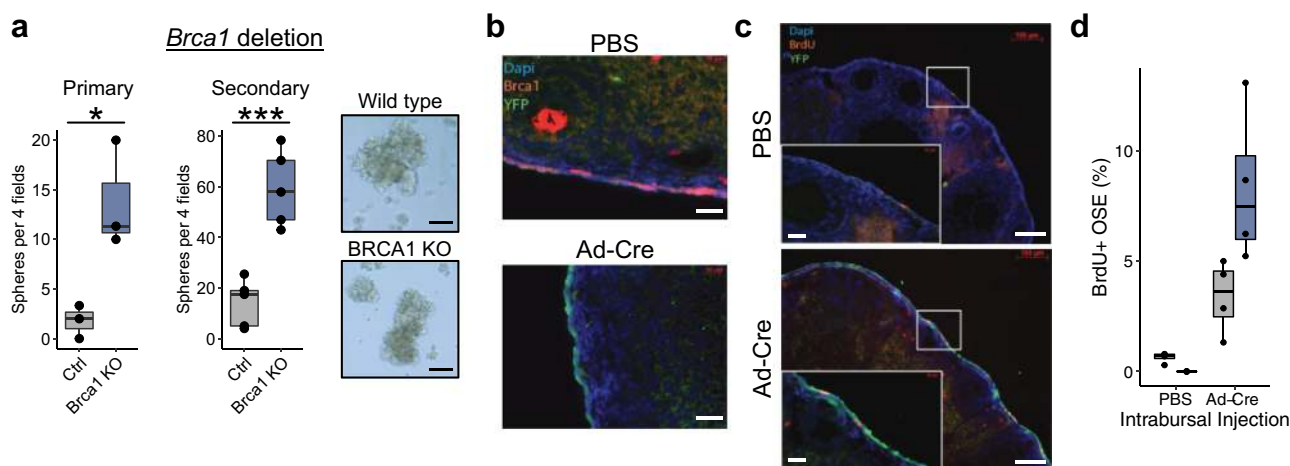


Fig. 5 *Brca1* deletion in vivo promotes increased label retention. **a** Primary (left; $n = 3$) and secondary (middle; $n = 5$) sphere forming capacity of mOSE cells following *Brca1* deletion by infection with Ad-Cre (*Brca1* KO). Cells infected with Ad-GFP were used as a control (Ctrl). Data points represent the average number of spheres per 4 fields of view for each replicate. Right: Phase contrast images of control (OSE from PBS-injected mice) and BRCA KO spheroids. Spheroids were cultured for 14 days. Scale bar = 100 μm . **b** Immunohistochemical staining of ovaries following intrabursal injection of PBS or Ad-Cre. Staining shows BRCA1 (red) and the YFP (green) reporter activated upon delivery of Cre recombinase. Nuclei are stained with DAPI (blue). Scale bar = 25 μm . **c** BrdU label retention (red) and YFP (green) signal in ovaries following intrabursal injection of either PBS or Ad-Cre. Scale bar = 100 μm , inset scale bar = 25 μm . **d** Quantification of BrdU+ OSE cells in ovaries ($n = 4$ ovaries from independent mice). All boxplots show median value (horizontal black line), estimated 25th and 75th percentiles, and whiskers represent 1.5 times the interquartile range.

crosstalk, activating growth factor signaling pathways, which we do not see in *Brca1*-null OSE cells.

Comparing the expression profiles of each condition associated with stemness phenotypes in this study, we find minimal overlap in the specific genes activated or repressed in each (Fig. 6d). Ranking genes by the number of conditions they are activated or repressed in, we found that *Adamts4* and *Pnmal2* are the only genes upregulated in all four conditions (Fig. 6e). *Adamts4* has been linked to stemness in uveal melanoma through modulating crosstalk between the cells and their adjacent ECM³⁰. While this may be relevant here, conserved downstream signals promoting stemness remain elusive. We note high frequency of EMT-associated changes, including activation of Snail, various collagens, and repression of cytokeratins (Fig. 6e). Notably, however, specific EMT transcription factors and putative OSE stemness markers (*Lgr5*, *Aldh1a1*, *Ly6a*, *Nanog*, and *Cd44*) are only activated in 1-2 conditions, and are even repressed in some conditions (Fig. 6e).

Discussion

Several studies have reported putative stem cell populations in the OSE, but the relationships between these populations are unclear. The ability of differentiated epithelial cells to dedifferentiate and fulfil functional roles of stem cells has now been observed in several tissues, suggesting that static stem cell populations may not be required to maintain all tissues. In this study, we have further explored the ability of OSE cells to acquire features of stemness and have demonstrated it can be promoted by a variety of conditions. It may be expected that a common gene expression program would underlie the specific stemness phenotype we have assessed with these experiments, but we demonstrate that expression profiles are context specific.

While transcriptional responses were variable, several patterns were recurrent across multiple conditions. We observed that induction of an EMT with TGF β 1 treatment or Snail overexpression could promote stemness in OSE, but expression profiles of spheroids naive to TGF β 1 treatment also showed EMT activation, which has also been observed with ovarian cancer cells

cultured as spheroids³¹. As spheroids have been shown to enrich for cells with stem cell properties, these findings suggest that intrinsic stemness— independent of exogenous treatments— may be associated with a more mesenchymal phenotype. The relationship between the EMT and stemness is well documented^{12,32}, but there is growing evidence that stemness and EMT are not inextricably linked. For example, the EMT-promoted transcription factor PRRX1 suppresses stemness in breast cancer cells³³. Further, transcriptional dynamics of the EMT have been shown to be highly context-specific, which explains why it does not consistently promote stemness²⁵. Just as the EMT can occur without promoting stemness, we have shown that deletion of *Brca1* promotes stemness in OSE without activating any EMT-associated expression, including *Twist1* activation, which had been shown to drive stemness following *Brca1* deletion in mammary epithelial cells²⁸. Instead, *Brca1* loss caused many changes in cell membrane transport and metabolic genes. While the mechanism of induced stemness following *Brca1* loss is unclear, this provides strong evidence that stemness is not dependent on a mesenchymal expression profile and is perhaps as context specific as the EMT response²⁵.

Several alterations in signaling pathway activity were also common across conditions. TGF β 1 treatment and spheroids were associated with higher levels of ERK activity, which have both been linked to stemness in epithelial³⁴ and carcinoma cells³⁵. In EGF-free media, paracrine/autocrine signaling is established, maintaining ERK activity in stem cell populations of intestinal organoids³⁵. While these mechanisms may contribute to stemness in OSE spheroids or those treated with TGF β 1, increased ERK activity was not enhanced following Snail overexpression or *Brca1* loss. Similarly, a gene set comprising interferon alpha response genes was downregulated following spheroid culture, TGF β 1 treatment, and Snail overexpression. While it is unlikely that interferon alpha itself was present, it is possible that various signaling pathways may affect common target genes. Consistent with this, disruption of type 1 interferon signaling promotes stemness in breast cancer cells³⁶. None of these patterns, however, are consistent across all conditions, further supporting that mechanisms promoting stemness may vary considerably

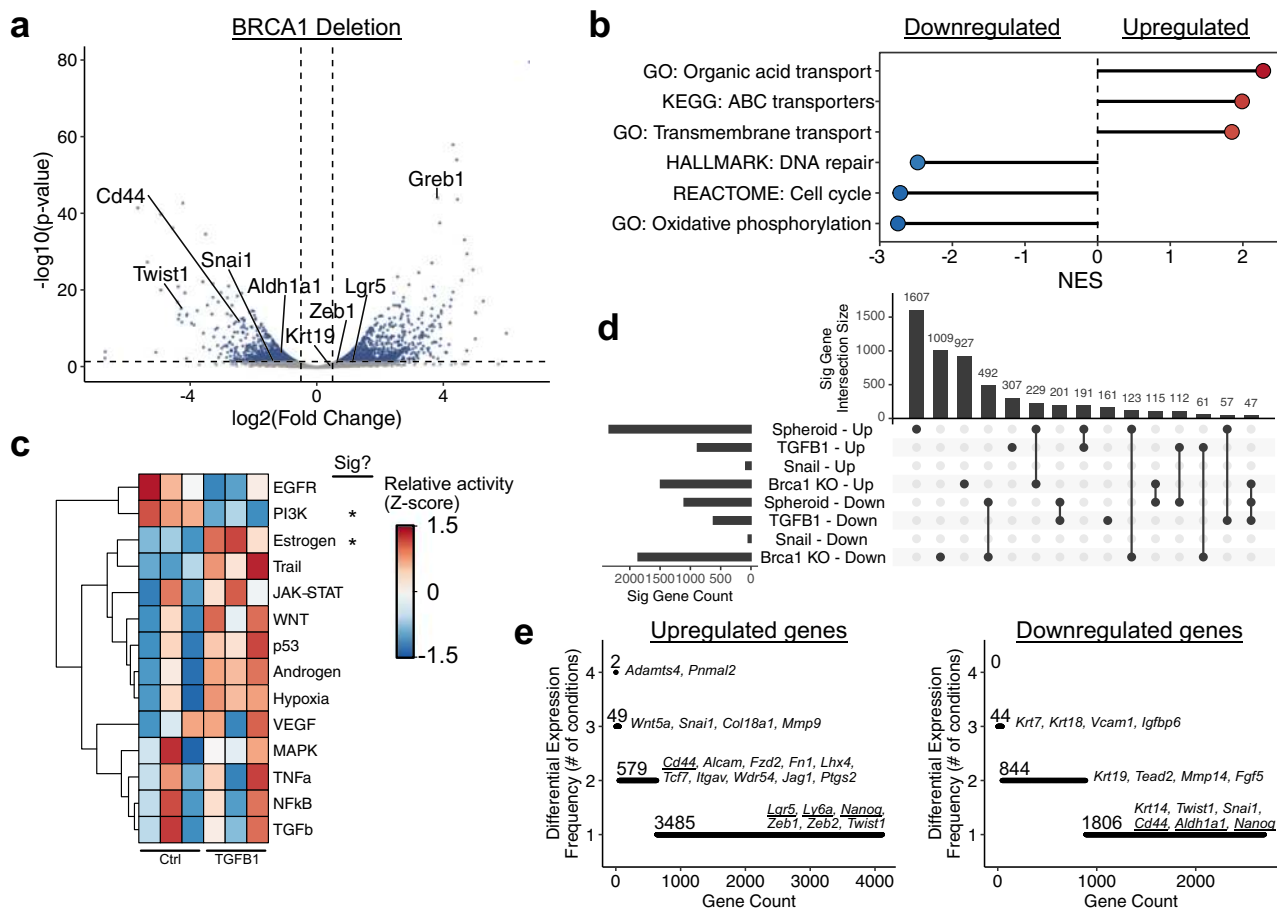


Fig. 6 Stemness phenotypes are transcriptionally diverse. **a** Plot showing the distribution of differentially expressed genes following *Brca1* deletion by infection with Ad-Cre. Each point corresponds to a single gene. Selected genes related to stemness and/or the EMT are highlighted on the plot. Dashed lines correspond to significance criteria (absolute log fold change >0.5, $p < 0.05$). **b** GSEA results for selected gene sets enriched in differentially expressed genes following *Brca1* deletion. All gene sets are significantly enriched ($p < 0.05$) and NES values are shown. **c** Inferred pathway activity in control and Snail-overexpressing mOSE cells. P -values were computed from the t statistic of a linear regression model and were adjusted using the Benjamini-Hochberg FDR method. **d** UpSet plot showing overlaps in differentially expressed genes between all conditions assessed ranked by the condition/overlap with the largest number of genes. **e** Plots showing the number of assessed conditions that genes are either activated or repressed in. Selected genes are listed and putative stemness markers are underlined.

depending on environmental conditions (e.g., ovulatory wound repair, tissue expansion during folliculogenesis, natural cell turnover).

While we have relied heavily on *in vitro* models here, this has enabled us to explore the ability of OSE cells to acquire stemness following various experimental perturbations. This suggests that differentiated epithelial cells may be capable of self-regulating tissue maintenance in response to environmental cues, such as tissue damage. The expression profiles of this emergent stemness may be variable, depending on the specific properties of the cells' microenvironment. This model is particularly interesting because it is a stark contrast to how stem cells and differentiation hierarchies have been viewed for the last several decades. The OSE is a promising tissue to explore this further as it undergoes regular rupture and repair throughout reproductive cycles, and is a simple tissue comprising a single cell type, which may be the most likely to exhibit this behavior. Designing strategies to monitor stemness dynamics *in vivo* will be critical to understand these behaviors in a normal physiological context.

Methods

OSE cell isolation and culture. The isolation and culture of mOSE cells was done as previously described¹⁰, in accordance with the guidelines of the Canadian

Council on Animal Care and under a protocol approved by the University of Ottawa Animal Care Committee. Briefly, ovaries from randomly cycling female mice (FVB/N, 6 weeks old) were collected and incubated in 0.25% Trypsin/PBS (Invitrogen) (37 °C, 5% CO₂, 30 min) to facilitate OSE removal. mOSE cells were isolated by centrifugation and plated onto tissue culture plates (Corning) in mOSE media [a-Minimum Essential Medium (Corning) supplemented with 4% FBS, 0.01 mg/mL insulin-transferrin-sodium-selenite solution (ITSS; Roche), and 2 µg/mL EGF (R&D Systems)]. hOSE cells were isolated and cultured as previously described³⁷, with patient consent and under a protocol approved by the Ottawa Health Science Network Research Ethics Board (Protocol #1999540). Briefly, ovaries from 5 different women were collected during surgery for reasons other than ovarian pathology. Using a scalpel, hOSE cells were scraped from the ovarian surface and isolated by centrifugation in hOSE media (Wisent Bioproducts) supplemented with 10% FBS. All mouse and human OSE cells were passaged 2–3 times prior to experimental use and experiments were conducted with cells of a passage number less than 25.

Quantitative reverse transcription polymerase chain reaction (RT-PCR). The RNeasy Mini Kit (Qiagen) was used to extract RNA and the OneStep RT-PCR Kit (Qiagen) was used to synthesize cDNA. Quantitative PCR was done using the ABI 7500 FAST qRT-PCR machine (Applied Biosystems) using the Taqman gene expression (Life Technologies) and SsoFast gene expression (Bio-rad) assays utilizing *Tbp* as an endogenous control. Primer sequences are listed in Supplemental Table 1. RQ (relative quantity) was determined using the cycling threshold for the gene of interest in control or untreated samples compared to the cycling threshold in experimental samples, calculated using the Applied Biosystems 7500 FAST v2.3 software.

Western blot. M-PER mammalian protein extraction reagent (GE Healthcare) was used to extract protein from mOSE cells and run on NuPAGE 4–12% Bis-Tris gradient gels (Life Technologies). Polyvinylidene difluoride membranes were used to transfer protein samples. Membranes were blocked in 5% non-fat milk prior to antibody incubation. Antibody conditions are described in Supplemental Table 2. Western blots were developed using Clarity™ Western ECL Substrate (Bio-Rad) and the FluorChem FC2 imaging system (Alpha Innotech).

Stem cell PCR array. mOSE cells (1×10^6 cells) were plated 24 h prior to treatment with TGFβ1 (10 ng/mL, R&D Systems). RNA was collected 7 days post TGFβ1 treatment (RNAeasy Kit, Qiagen). cDNA synthesis was performed using RT² First Strand Kit (Qiagen) and run on the RT² First Strand Kit (Stem cell PCR array) (Qiagen). The array was run in triplicate ($N = 3$) and analyzed using the DataAnalysis Excel platform provided with the array kits.

Snail-overexpressing mOSE cells. mOSE cells stably expressing reverse tetracycline-controlled transactivator (rtTA) protein were transduced with a lentiviral construct (pWPI) expressing the murine *Snail* or *eGFP* under the control of a doxycycline-inducible promoter and the hygromycin resistance gene under the control of the *PGK* promoter. Transduced cells were selected for resistance to Hygromycin B. 200 ng/mL of doxycycline was added to cultures for 4 days prior to all experiments overexpressing Snail.

Primary sphere-forming assays. For free-floating spheres, mOSE cells were cultured in stem cell media [Dulbecco's Modified Eagle's Medium: Nutrient Mixture F-12 (Sigma) supplemented with 1 X B27 supplement (Invitrogen), 0.02 μg/mL EGF (R&D Systems), 0.04 μg/mL fibroblast growth factor (FGF; R&D Systems), 4 μg/mL heparin (Sigma) and 0.01 mg/mL ITSS (Roche), and 2 μg/mL EGF (R&D Systems)] at 5×10^4 cells/mL in non-adherent 24-well culture plates (Corning) and incubated at 37 °C, 5% CO₂ for 14 days. For TGFβ1-treated spheres, cells were pre-treated with recombinant TGFβ1 (10 ng/mL) for 4 days prior to being placed in spheroid culture and was replenished when plating cells in spheroid culture. Spheres were quantified using ImageJ using a pixel cutoff of >1000 pixels and a circularity limit of 0.5–1.0. For spheres cultured in methylcellulose, mOSE cells were placed in a 1:1 mixture of methylcellulose and stem cell media at 5×10^4 cells/mL in 24-well culture plates (Corning), and incubated at 37 °C, 5% CO₂ for 28 days. Methylcellulose-embedded spheres were quantified using ImageJ using a pixel cutoff of >500 pixels and a circularity limit of 0.5–1.0. For each experiment, a minimum of 3 replicates were performed, each replicate was performed in three independent wells, spheres were counted in 4 fields per well, and the average count was reported.

Secondary sphere-forming assay. Primary free-floating mOSE spheres were collected and washed in PBS. Spheres were dissociated by first incubating in trypsin/PBS (Invitrogen) at 37 °C for 10 min, then by passing cells through a 25 gauge needle to obtain a single cell suspension. Single cell suspension was verified using phase contrast microscopy. Cells were washed in PBS, counted using a hemocytometer, and plated in stem cell media at 5×10^4 cells/mL. Cells were incubated in non-adherent 24-well culture plates (Corning) at 37 °C, 5% CO₂ for 14 days. Spheres were quantified using ImageJ using a pixel cutoff of >500 pixels and a circularity limit of 0.5–1.0.

Spheroid immunofluorescence. Control and TGFβ1-treated spheroids were collected after 14 days in free-floating spheroid culture, and fixed in 4% paraformaldehyde for 30 min. Spheroids were then embedded in Eprelia HistoGel Embedding Media prior to being transferred into 70% ethanol overnight. HistoGel blocks were then embedded in paraffin. Paraffin were sectioned at 5 μm and dried overnight on slides at room temperature. Sections were deparaffinized in Xylene and rehydrated in a series of graded ethanol baths. Antigen retrieval and permeabilization was performed using heat-mediated antigen unmasking solution (H-3300, Vector Laboratories, Burlingame, Ca, USA) according to manufacturer's instructions followed by incubations in 0.2% Triton X-100 diluted in PBS for 15 min at room temperature, respectively. Slides were rinsed three times PBS-T and incubated in blocking solution [10% goat serum (G9023, Sigma-Aldrich, St. Louis, MS, USA) with 1% BSA diluted in PBS] for 30 min at room temperature followed by an overnight incubation at 4 °C in primary antibodies [rabbit anti-Ki-67 (ab9260, MilliporeSigma, Burlington, MA, USA) at 1:50 and rat anti-Cd44 (ab119348, Abcam, Cambridge, UK) at 1:100 diluted in blocking buffer]. Slides were rinsed three times in PBS-T and incubated in 1:200 dilution of secondary antibodies in blocking buffer [Goat anti-Rabbit IgG AlexaFluor 488 (A-11006, Invitrogen, Carlsbad, CA, USA) and Goat anti-Rat IgG AlexaFluor 594 (A-11012, Invitrogen, Carlsbad, CA, USA)] for 1 h at room temperature and wash three times with PBS. The slides were mounted with ProLong™ Diamond Antifade Mountant with DAPI (P36962, ThermoFisher, Waltham, MA, USA) and coverslip. We used the Zeiss Axioskop 2 MOT (Oberkochen, Germany) fluorescence imaging microscope at 20x and 40x magnification. Intensity thresholds were set according to the highest intensity image and a minimum of three images was analyzed for each treatment ($n = 3$).

Brca1 deletion in mOSE cells. mOSE cells were isolated from homozygous *Brca1^{tm1Brn}* mice as described above and then infected with Ad-Cre to achieve *Brca1* knockout. Ad-GFP was used as a control. Cells were cultured for 1 week after infection prior to experimental use.

BrdU pulse-chase. *Brca1^{tm1Brn}* mice were bred to *B6.129×1-Gt(ROSA)26Sor^{tm1}(EYFP)^{Cos/}* mice to produce *Brca1^{fl/yf}YFP* mice. Six week-old *Brca1^{fl/yf}YFP* mice were injected IB with Ad-Cre (8×10^7 PFU) or PBS on day 1 and injected IP with BrdU (0.25 mg daily) on days 7–10. Ovaries were collected on day 40 and frozen in Optimal Cutting Temperature Compound.

BrdU immunofluorescence. Frozen sections (5 μm) were fixed using formalin-vapor fixation³⁸ overnight at –20 °C. Samples were then hydrated in PBS and antigen retrieval performed using an antigen unmasking solution (pH 6.0, Vector) in a steam chamber (Hamilton Beach). Slides were then washed in PBS and blocked with 5% goat serum for 1 h at room temperature. Primary antibodies against BRCA1 (1:200, H-300, rabbit), GFP (1:1000, ab13970, chicken), and BrdU (1:200, ab6326, rat) were added and incubated overnight at 4 °C. Following a PBS wash, species-appropriate secondary antibodies (1:250, Alexafluor 594 nm or 488 nm) were incubated for 1 h at room temperature. Slides underwent a final PBS wash and were mounted using Prolong Gold with DAPI (ThermoFisher). Quantifications of BrdU+ cells were performed by taking cross-sections of ovaries and manually counting OSE nuclei (DAPI) around the perimeter of the tissue. Experimenters were blinded to the experimental group of each tissue section and YFP channel was not shown during quantification.

RNA-seq sample preparation. For TGFβ1 treatment of monolayer cultures, mOSE cells were plated 24 h prior to the addition of TGFβ1 (10 ng/mL, R&D Systems) and cells were collected after 4 days of treatment. For inducible *Snail* expression and *Brca1* deletion, cells were plated for 24 h prior to the addition of doxycycline (200 ng/mL, Sigma), and RNA was collected 4 days later. For sphere-forming conditions, mOSE cells (1×10^6) were first plated as monolayer cultures 24 h prior to treatment with TGFβ1 (10 ng/mL, R&D Systems). Four days after the addition of TGFβ1, mOSE cells were then plated in free-floating sphere-forming conditions. Cells were maintained in sphere-forming cultures for 2 weeks prior to RNA collection (RNAeasy Kit, Qiagen). TGFβ1 was replenished when placing mOSE cells in sphere-forming conditions.

Library preparation and sequencing. Total RNA was quantified using a NanoDrop Spectrophotometer ND-1000 (NanoDrop Technologies, Inc.) and its integrity was assessed on a 2100 Bioanalyzer (Agilent Technologies). Libraries were generated from 250 ng of total RNA as follows: mRNA enrichment was performed using the NEBNext Poly(A) Magnetic Isolation Module (New England BioLabs). cDNA synthesis was achieved with the NEBNext RNA First Strand Synthesis and NEBNext Ultra Directional RNA Second Strand Synthesis Modules (New England BioLabs). The remaining steps of library preparation were done using the NEBNext Ultra II DNA Library Prep Kit for Illumina (New England BioLabs). Adapters and PCR primers were purchased from New England BioLabs. Libraries were quantified using the Quant-iT™ PicoGreen® dsDNA Assay Kit (Life Technologies) and the Kapa Illumina GA with Revised Primers-SYBR Fast Universal kit (Kapa Biosystems). Average size fragment was determined using a LabChip GX (PerkinElmer) instrument.

The libraries were normalized, denatured in 0.05 N NaOH, and then diluted to 200 pM and neutralized using HT1 buffer. ExAMP was added to the mix and the clustering was done on an Illumina cBot and the flowcell was run on a HiSeq 4000 for 2×100 cycles (paired-end mode) following the manufacturer's instructions. A phiX library was used as a control and mixed with libraries at 1% level. The Illumina control software was HCS HD 3.4.0.38 and the real-time analysis program was RTA v. 2.7.7. The program bcl2fastq2 v2.18 was then used to demultiplex samples and generate fastq reads.

RNA-seq processing and differential expression. Transcript quantification for each sample was performed using kallisto (v0.45.0)³⁹ with the GRCm38 transcriptome reference and the –b 50 bootstrap option. The R package Sleuth (v0.30.0)⁴⁰ was then used to construct general linear models for the log-transformed expression of each gene across experimental conditions. Wald's test was used to test for significant variables for each gene and the resultant *p*-values were adjusted to *q*-values using the Benjamini–Hochberg false discovery rate method. Significant genes were defined as genes with a *q*-value <0.05. An effect size (beta coefficient of the regression model) cutoff of >0.5 or < –0.5 was also used for each data set. To compare TGFβ1-treated spheres with monolayer conditions and the untreated spheroids, we used a regression model including an interaction term between spheroid culture and TGFβ1 treatment to identify expression patterns associated with TGFβ1-treated spheres that are not simply additive changes due to the two variables.

Gene set enrichment analysis and pathway activity inference. GSEA was performed with the R package fgsea (v1.13.5)⁴¹. GO terms, KEGG pathways,

Reactome pathways, and Hallmark genesets were collected from the Molecular Signatures Database (MSigDB)^{22,23} and used to query differential expression results ranked by fold change. All gene sets discussed in the manuscript have a significant enrichment (Benjamini–Hochberg adjust p -value <0.05). For pathway activity inference, we used the R package PROGENy (v1.9.6)⁴². Pathway activity was compared between experimental conditions using a simple linear model and p -values were adjusted using the Benjamini–Hochberg false detection rate method.

CD44 cell sorting. mOSE cells were treated with TGF β 1 (10 ng/mL, 2 days) prior to collecting cells for FACS. Cells (1×10^7) were trypsinized and a single-cell suspension was made using a 40 μ m cell strainer. Cells were labeled and sorted as previously described¹⁸. Briefly, cells were resuspended in a flow buffer (4% FBS in PBS) and incubated with anti-CD44 conjugated to allophycocyanin (1:5000; eBioscience, San Diego, CA) for 15 min at 4 °C. Unbound antibody was removed with washing buffer and the fraction of cells with surface protein labeled with CD44 antibody was determined using a MoFlo cell sorter (Dako Cytomation).

Statistics and reproducibility. Statistical analyses were conducted in R (v4.0.3). For all comparisons of means, data were assessed with linear models and two-sided Student's t tests. For experiments involving multiple comparisons, p -values were controlled using the Benjamini–Hochberg false discovery rate method. To ensure reproducibility, all experiments were conducted with independent biological replicates. The number of replicates are specified in figure legends. Individual values for data plots are included in the public GitHub repository at https://github.com/dpcook/ose_stemness.

Reporting summary. Further information on research design is available in the Nature Research Reporting Summary linked to this article.

Data availability

Raw sequencing files have been deposited and are available along with processed transcript quantifications at GSE122875. Source data for all plots in main figures is provided with this paper.

Code availability

All code used to process data and generate figures is available in a public GitHub repository⁴³. Code can be viewed at https://github.com/dpcook/ose_stemness.

Received: 15 June 2020; Accepted: 26 March 2021;

Published online: 05 May 2021

References

- Barker, N., van de Wetering, M. & Clevers, H. The intestinal stem cell. *Genes Dev.* **22**, 1856–1864 (2008).
- Tata, P. R. et al. Dedifferentiation of committed epithelial cells into stem cells in vivo. *Nature* **503**, 218–223 (2013).
- Herrick, S. E. & Mutsaers, S. E. The potential of mesothelial cells in tissue engineering and regenerative medicine applications. *Int. J. Artif. Organs* **30**, 527–540 (2007).
- Singavarapu, R., Buchinsky, N., Cheon, D. J. & Orsulic, S. Whole ovary immunohistochemistry for monitoring cell proliferation and ovulatory wound repair in the mouse. *Reprod. Biol. Endocrinol.* **8**, 98 (2010).
- Murdoch, W. J. Ovarian surface epithelium during ovulatory and anovulatory ovine estrous cycles. *Anat. Rec.* **240**, 322–326 (1994).
- Bjersing, L. & Cajander, S. Ovulation and the role of the ovarian surface epithelium. *Experientia* **31**, 605–608 (1975).
- Wright, J. W., Jurevic, L. & Stouffer, R. L. Dynamics of the primate ovarian surface epithelium during the ovulatory menstrual cycle. *Hum. Reprod.* **26**, 1408–1421 (2011).
- Ng, A. & Barker, N. Ovary and fimbrial stem cells: biology, niche and cancer origins. *Nat. Rev. Mol. Cell Biol.* **16**, 625–638 (2015).
- Auersperg, N. The stem-cell profile of ovarian surface epithelium is reproduced in the oviductal fimbriae, with increased stem-cell marker density in distal parts of the fimbriae. *Int. J. Gynecol. Pathol.* **32**, 444–453 (2013).
- Gamwell, L. F., Collins, O. & Vanderhyden, B. C. The mouse ovarian surface epithelium contains a population of LY6A (SCA-1) expressing progenitor cells that are regulated by ovulation-associated factors. *Biol. Reprod.* **87**, 80 (2012).
- Flesken-Nikitin, A. et al. Ovarian surface epithelium at the junction area contains a cancer-prone stem cell niche. *Nature* **495**, 241–245 (2013).
- Mani, S. A. et al. The epithelial-mesenchymal transition generates cells with properties of stem cells. *Cell* **133**, 704–715 (2008).
- Haensel, D. & Dai, X. Epithelial-to-mesenchymal transition in cutaneous wound healing: where we are and where we are heading. *Dev. Dyn.* **247**, 473–480 (2018).
- Shaw, T. J. & Martin, P. Wound repair: a showcase for cell plasticity and migration. *Curr. Opin. Cell Biol.* **42**, 29–37 (2016).
- Knight, P. G. & Glicker, C. TGF- β superfamily members and ovarian follicle development. *Reproduction* **132**, 191–206 (2006).
- Carter, L. E. et al. COX2 is induced in the ovarian epithelium during ovulatory wound repair and promotes cell survival. *Biol. Reprod.* **101**, 961–974 (2019).
- Hebbard, L. et al. CD44 expression and regulation during mammary gland development and function. *J. Cell Sci.* **113**, 2619–2630 (2000). (Pt 14).
- Alwosabai, K. et al. PAX2 maintains the differentiation of mouse oviductal epithelium and inhibits the transition to a stem cell-like state. *Oncotarget* **8**, 76881–76897 (2017).
- Herheliuk, T., Perepelytsina, O., Ugnivenko, A., Ostapchenko, L. & Sydorenko, M. Investigation of multicellular tumor spheroids enriched for a cancer stem cell phenotype. *Stem Cell Investig.* **6**, 21 (2019).
- Robertson, F. M. et al. Imaging and analysis of 3D tumor spheroids enriched for a cancer stem cell phenotype. *J. Biomol. Screen.* **15**, 820–829 (2010).
- Liao, M.-J. et al. Enrichment of a population of mammary gland cells that form mammospheres and have in vivo repopulating activity. *Cancer Res.* **67**, 8131–8138 (2007).
- Subramanian, A. et al. Gene set enrichment analysis: a knowledge-based approach for interpreting genome-wide expression profiles. *Proc. Natl Acad. Sci. U.S.A.* **102**, 15545–15550 (2005).
- Liberzon, A. et al. The Molecular Signatures Database (MSigDB) hallmark gene set collection. *Cell Syst.* **1**, 417–425 (2015).
- Luo, K. Signaling Cross Talk between TGF- β /Smad and Other Signaling Pathways. *Cold Spring Harb. Perspect. Biol.* **9**, a022137 (2017).
- Cook, D. P. & Vanderhyden, B. C. Context specificity of the EMT transcriptional response. *Nat. Commun.* **11**, 1–9 (2020).
- Tacha, D., Zhou, D. & Cheng, L. Expression of PAX8 in normal and neoplastic tissues: a comprehensive immunohistochemical study. *Appl. Immunohistochem. Mol. Morphol.* **19**, 293–299 (2011).
- Hodgkinson, K. et al. GREB1 is an estrogen receptor-regulated tumour promoter that is frequently expressed in ovarian cancer. *Oncogene* **37**, 5873–5886 (2018).
- Bai, F. et al. BRCA1 suppresses epithelial-to-mesenchymal transition and stem cell dedifferentiation during mammary and tumor development. *Cancer Res.* **74**, 6161–6172 (2014).
- Di Zazzo, E. et al. Estrogen receptors in epithelial-mesenchymal transition of prostate cancer. *Cancers* **11**, 1418 (2019).
- Peris-Torres, C. et al. Extracellular protease ADAMTS1 is required at early stages of human uveal melanoma development by inducing stemness and endothelial-like features on tumor cells. *Cancers* **12**, 801 (2020).
- Rafehi, S. et al. TGF β signaling regulates epithelial-mesenchymal plasticity in ovarian cancer ascites-derived spheroids. *Endocr. Relat. Cancer* **23**, 147–159 (2016).
- Wilson, M. M., Weinberg, R. A., Lees, J. A. & Guen, V. J. Emerging mechanisms by which EMT programs control stemness. *Trends Cancer Res.* <https://doi.org/10.1016/j.trecan.2020.03.011> (2020).
- Ocaña, O. H. et al. Metastatic colonization requires the repression of the epithelial-mesenchymal transition inducer Prrx1. *Cancer Cell* **22**, 709–724 (2012).
- Beumer, J. & Clevers, H. Regulation and plasticity of intestinal stem cells during homeostasis and regeneration. *Development* **143**, 3639–3649 (2016).
- Brandt, R. et al. Cell type-dependent differential activation of ERK by oncogenic KRAS in colon cancer and intestinal epithelium. *Nat. Commun.* **10**, 2919 (2019).
- Castiello, L. et al. Disruption of IFN-I signaling promotes HER2/Neu tumor progression and breast cancer stem cells. *Cancer Immunol. Res.* **6**, 658–670 (2018).
- Tonary, A. M., Macdonald, E. A., Faught, W., Senterman, M. K. & Vanderhyden, B. C. Lack of expression of c-KIT in ovarian cancers is associated with poor prognosis. *Int. J. Cancer* **89**, 242–250 (2000).
- Jockusch, H., Voigt, S. & Eberhard, D. Localization of GFP in frozen sections from unfixed mouse tissues: immobilization of a highly soluble marker protein by formaldehyde vapor. *J. Histochem. Cytochem.* **51**, 401–404 (2003).
- Bray, N. L., Pimentel, H., Melsted, P. & Pachter, L. Near-optimal probabilistic RNA-seq quantification. *Nat. Biotechnol.* **34**, 525–527 (2016).
- Pimentel, H., Bray, N. L., Puente, S., Melsted, P. & Pachter, L. Differential analysis of RNA-seq incorporating quantification uncertainty. *Nat. Methods* **14**, 687–690 (2017).
- Korotkevich, G., Sukhov, V. & Sergushichev, A. Fast gene set enrichment analysis. Preprint at *bioRxiv* <https://doi.org/10.1101/060012>.
- Schubert, M. et al. Perturbation-response genes reveal signaling footprints in cancer gene expression. *Nat. Commun.* **9**, 20 (2018).
- Cook, D. P. dpcook/ose_stemness: comms_bio_release, v1.0. Zenodo, <https://doi.org/10.5281/zenodo.4610521>.

Acknowledgements

We thank the tissue donors for making this research possible. We also thank Dr. Ken Garson for generating mOSE cells with inducible *Snail* and inducible *GFP* expression, and Dr. Diane Lagacé for providing *B6.129×1-Gt(ROSA)26Sor^{tm1(EYFP)Cosy/J}* mice. We wish to acknowledge the contribution of staff of the McGill University and G enome Qu ebec Innovation Centre (Montreal, QC) for performing library preparation and sequencing associated with RNA-seq experiments. We also wish to acknowledge Stem-Core Laboratories (Ottawa, ON) for performing the FACS of CD44-positive mOSE cells. This work was supported by grants from the Canadian Institutes of Health Research and the National Science and Engineering Research Council (BCV). L.E.C. and L.F.G. were supported by Ontario Graduate Scholarships, D.P.C. by a Frederick Banting and Charles Best Doctoral Award (CIHR), and C.W.M. by the Vanier Canada Graduate Scholarship.

Author contributions

L.E.C. and B.C.V. conceived the study. L.E.C., D.P.C., and B.C.V. interpreted results and wrote the manuscript. L.E.C., M.A.G., L.F.G., O.C., H.A.D., and T.D. performed cell culture experiments, qPCR analysis, and Western blots. C.W.M. and D.A.L. performed immunofluorescence and its analysis. O.C. derived mOSE and hOSE cultures. C.W.M. performed mouse experiments. D.P.C. and L.E.C. performed all computational analysis.

Competing interests

The authors declare no competing interests.

Additional information

Supplementary information The online version contains supplementary material available at <https://doi.org/10.1038/s42003-021-02045-w>.

Correspondence and requests for materials should be addressed to B.C.V.

Reprints and permission information is available at <http://www.nature.com/reprints>

Publisher's note Springer Nature remains neutral with regard to jurisdictional claims in published maps and institutional affiliations.



Open Access This article is licensed under a Creative Commons Attribution 4.0 International License, which permits use, sharing, adaptation, distribution and reproduction in any medium or format, as long as you give appropriate credit to the original author(s) and the source, provide a link to the Creative Commons license, and indicate if changes were made. The images or other third party material in this article are included in the article's Creative Commons license, unless indicated otherwise in a credit line to the material. If material is not included in the article's Creative Commons license and your intended use is not permitted by statutory regulation or exceeds the permitted use, you will need to obtain permission directly from the copyright holder. To view a copy of this license, visit <http://creativecommons.org/licenses/by/4.0/>.

  The Author(s) 2021